Front. Chem. Sci. Eng. 2022, 16(11): 1632−1642
https://doi.org/10.1007/s11705-022-2187-6

RESEARCH ARTICLE

A ternary mechanism for the facilitated transfer of metal ions onto metal–organic frameworks: implications for the "versatility" of these materials as solid sorbents

Xiyuan Bu[1*], Ming Tian[1,2*], Hongqing Wang[2], Lin Wang[1], Liyong Yuan (✉)[1], Weiqun Shi[1]

1 Laboratory of Nuclear Energy Chemistry, Institute of High Energy Physics, Chinese Academy of Sciences, Beijing 100049, China
2 School of Chemistry and Chemical Engineering, University of South China, Hengyang 421001, China

© Higher Education Press 2022

Abstract Although metal–organic frameworks offer a new platform for developing versatile sorption materials, yet coordinating the functionality, structure and component of these materials remains a great challenge. It depends on a comprehensive knowledge of a "real sorption mechanism". Herein, a ternary mechanism for U(VI) uptake in metal–organic frameworks was reported. Analogous MIL-100s (Al, Fe, Cr) were prepared and studied for their ability to sequestrate U(VI) from aqueous solutions. As a result, MIL-100(Al) performed the best among the tested materials, and MIL-100(Cr) performed the worst. The nuclear magnetic resonance technique combined with energy-dispersive X-ray spectroscopy and zeta potential measurement reveal that U(VI) uptake in the three metal–organic frameworks involves different mechanisms. Specifically, hydrated uranyl ions form outer-sphere complexes in the surface of MIL-100s (Al, Fe) by exchanging with hydrogen ions of terminal hydroxyl groups (Al-OH_2, Fe-OH_2), and/or, hydrated uranyl ions are bound directly to Al(III) center in MIL-100(Al) through a strong inner-sphere coordination. For MIL-100(Cr), however, the U(VI) uptake is attributed to electrostatic attraction. Besides, the sorption mechanism is also pH and ionic strength dependent. The present study suggests that changing metal center of metal–organic frameworks and sorption conditions alters sorption mechanism, which helps to construct effective metal–organic frameworks-based sorbents for water purification.

Keywords U(VI), metal–organic frameworks, adsorption mechanism, metal node

Received April 12, 2022; accepted May 14, 2022

E-mail: yuanly@ihep.ac.cn

* These authors contributed equally to this work.

1 Introduction

Due to ever-increasing global energy consumption and the increasingly prominent environmental issues in recent years, it is increasingly urgent to find new non-fossil energy sources [1]. Nuclear power is considered a "clean energy" in view of none emission of greenhouse gases and extremely high energy density that can meet the growing energy demand of humanity [2,3]. At the same time, however, various ecotoxic radionuclides from the nuclear fuel cycle are released into the environment, which causes a huge negative effect on the environment and humanity health [4]. Therefore, novel materials and technologies are anticipated to improve the nuclear fuel cycle [5,6]. In particular, novel sorbents are critically needed to extract uranium from waste streams and acid mine drainages [7–9]. As such, a number of solid-phase sorbents, such as porous carbon [10,11], metal oxides [12], graphene oxides [13–15], and layered double hydroxides [16,17], have been developed over the last decades for the uptake of the radionuclides. Among these sorbents, metal–organic frameworks (MOFs), also known as porous coordination polymer, are becoming a new favorite. MOFs are highly porous hybrid crystalline solids consisting of central metal ions or clusters and organic linkers. As emerging materials with extraordinary porosity, tunable composition and excellent chemical and structure stability resulting from the combined impacts of their organic and inorganic moieties, MOFs are gaining immense attention and showing a range of promising applications in gas storage [18,19], separations [20–22], sensing [23], catalysis [24], and drug delivery [25]. Moreover, these porous structures with pores of molecular dimensions are associated with a series of desirable properties such as low density, ultrahigh surface area to mass ratio. Recently, MOFs as sorbents of

radionuclides have been reported by us and others. Lin et al. [26], for example, reported the highly porous Zr-based MOFs UiO-68-(NH)(PO)$(OEt)_2$ for U(VI) extraction. The experimental results confirm that the MOFs can effectively adsorb U(VI) and the saturation capacity reaches 217 $mg \cdot g^{-1}$ from water at pH = 2.5. Derivatives of MIL-101 were utilized as sorbents to remove U(VI) from water [27]. Amine functional groups on the frameworks of MIL-101(Cr) greatly enhance the U(VI) uptake onto the MOFs. Moreover, we reported, for the first time, a highly efficient Th(IV) sorption with the carboxyl derivatives of UiO-66 [28]. These results clearly present opportunities for separating MOFs in radionuclides from wastewater. Up to now, however, the questions of whether or not the structure and component of MOFs correlates with their adsorbability and selectivity towards certain radionuclides has been rarely addressed. Very recently, we have published a study on defect engineering of UiO-66 with more active binding sites and more open frameworks for U(VI) capture from wastewater [29]. It is found that tailoring missing-linker defects drastically improves U(VI) uptake in the MOFs. In this work, another key issue affecting U(VI) uptake in MOFs has been addressed, i.e., metal node. Several studies have already proven that the adsorption properties of porous isostructural MOFs can be greatly changed by modulating center metals/clusters. Yoon et al. [30] for example, proposed that very large differences in N_2 adsorption occurred among the MIL-100(Cr), MIL-100(Al) and MIL-100(Fe) MOFs. Tong et al. [31] reported that MIL-100s (Fe, Cr) show very different dye capture behaviors. MIL-100(Fe) can efficiently capture both the anionic methyl orange (MO) and the cationic methylene blue (MB) with rapid kinetics simultaneously, while MIL-100(Cr) can selectively adsorb MB from an equal mass MO-MB mixture. All of these works demonstrated metal node effect on the adsorption properties of MOFs. Although our recent work [32] had revealed the influence of metal node on U(VI) uptake into MOFs, no data on the metal ions adsorption has been published.

The work aims to characterize the relationship between the metal nodes of MOFs and the mechanism of MOFs in the realm of solid phase extraction of metal ions. To achieve this aim, several analogous MOFs MIL-100s (Fe, Cr, Al) were prepared and explored as sorbents to sequestrate U(VI) from aqueous solution. U(VI) uptake in these MOFs as a function of various parameters such as time, pH, U(VI) concentration and ionic strength was investigated in detail, and the results were carefully compared. The mechanism of the U(VI) uptake in the MOFs was studied in-depth based on nuclear magnetic resonance (NMR), energy-dispersive X-ray spectroscopy (EDS), and zeta potential measurement. According to the above results, U(VI) uptake differs significantly in these MOFs, and metal nodes play a critical role in affecting the sorption mechanism of U(VI) into MOFs.

2 Experimental

2.1 Synthesis of MIL-100s (Fe, Cr, Al)

MIL-100s (Al, Fe, Cr) were prepared according to the protocol from the previously reported works [33–35] with some modifications in synthesis condition. Specially, MIL-100(Al) was prepared in a teflon-lined autoclave (100 mL) by mixing $Al(NO_3)_3 \cdot 9H_2O$ (1.74 g), trimethyl-1,3,5-benzenetricarboxylate (0.78 g), and 4 $mol \cdot L^{-1}$ HNO_3 (1.55 mL) in deionized water (25.2 mL). The initial pH was adjusted to 0.57 using HNO_3 solution, and the final pH was 1.85. The mixture was heated at 433 K for 12 h. After cooling, filtration, twice wash with water, and drying at room temperature, the yellowish product was obtained.

MIL-100(Fe) was prepared by mixing $Fe(NO_3)_3 \cdot 9H_2O$ (2.424 g) and trimesic acid (0.84 g) in water (6 mL). The reaction mixture was heated at 433 K for 12 h in a teflon-lined autoclave, and the final pH was 0.04. The product was collected following filtration, twice wash with water, and drying at room temperature.

MIL-100(Cr) was prepared by mixing CrO_3 (0.5 g), trimesic acid (1.05 g), and 5 $mol \cdot L^{-1}$ hydrofluoric acid solution (1.0 mL) in deionized water (24 mL). The slurry was stirred for a few minutes at room temperature and then decanted into a teflon-lined autoclave (100 mL) at 493 K for 96 h. The resulting green solid was washed with deionized water and ethanol and dried at room temperature under air atmosphere. To remove both the possible excess of metal ions and unreacted ligand, all the MOFs were washed in hot water at 343 K for 6 h and in hot ethanol at 343 K for 4 h, respectively.

2.2 Characterization of MIL-100s (Fe, Cr, Al)

The crystallinity was tested by powder X-ray diffraction (PXRD) with a Bruker AXS-D8 Advance diffractometer with a graphite monochromator, operating with Cu-Kα (λ = 1.541 Å, 40.0 kV, 40.0 mA) radiation in Bragg–Brentano geometry. The microstructures of the MOFs were characterized by a field-emission scanning electron microscope (Hitachi S-4800, Japan), and the chemical component analysis was performed by EDS (Horiba7593-H model). The zeta potentials were measured by dynamic light scattering method using a Zetasizer Nano ZS90 (Malvern Instruments, UK) over a pH range of 2.0 to 7.0. Thermogravimetric analysis (TGA) was carried out in air atmosphere with a heating rate of 10 $°C \cdot min^{-1}$. N_2 adsorption/desorption isotherms at 77 K were measured with an ASAP 2020 (Micromeritics). Prior to sorption measurements, the MIL-100(M) samples were outgassed for 6 h at 523 K with a turbo molecular pump vacuum. The Brunauer–Emmett–Teller (BET) area was determined from adsorption data in the relative pressure range from 0.03 to 0.2 using the BET equation. The total pore volume

was calculated from the amount adsorbed at a relative pressure of 0.97 and the pore size distribution was obtained using the non-local density functional theory method. The ^{27}Al magic angle spinning NMR spectra were obtained at a resonance frequency of 130.3 MHz using a Bruker Avance 500 MHz spectrometer. Chemical shifts are referenced to 1 mol·L^{-1} aqueous $Al(NO_3)_3$.

2.3 Batch sorption studies

U(VI) uptake in MIL-100(M) was performed by batch method at room temperature using 25 mL beaker. The effect of initial U(VI) concentration, equilibrium time, pH, temperature, ionic strength and competing ions were examined in detail. The U(VI) concentration used was within the range of 5–200 mg·L^{-1}. The solution pH was adjusted using 0.1 mol·L^{-1} HNO_3 or NaOH solution, and the ionic strength was controlled by adding a required amount of $NaClO_4$. The detailed experimental conditions are presented in the related figure captions for clear identification. The solutions were withdrawn from the flasks and separated from the solids by centrifugation. Then the initial and the residual concentration of tested ion(s) in supernatants were determined by inductively coupled plasma optical emission spectroscopy (Horiba Jobin Yvon). The uptake amount (Q_e, mg·g^{-1}) of metal ions and the distribution coefficient K_d are calculated as:

$$Q_e = \frac{(C_0 - C_e) \times V}{m}, \quad (1)$$

$$K_d = \frac{C_0 - C_e}{C_e} \times \frac{V}{m}, \quad (2)$$

where C_0 (mg·L^{-1}) is the initial concentration of metal ion, C_e (mg·L^{-1}) is the equilibrium concentration, V (L) is the volume of the testing solution and m (g) is sorbent dose. The solid–liquid experiment was repeated at least three times for each adsorption data with the uncertainty within 5%.

3 Results and discussion

3.1 Structural description of MIL-100s (Al, Cr, Fe)

MIL-100(M) (M = Al, Cr, Fe) is a metal(III) carboxylate built from trimers of metal octahedral sharing one oxygen atom and linked by rigid trimesate ligands (Fig. S1, cf. Electronic Supplementary Material, ESM). Each M_3O node in MIL-100s (Al, Cr, Fe) is connected to six ligands and each node possess three coordination unsaturated sites (CUS). To complete the metal-coordination sphere, the terminal hydroxyl group or water molecule or F element is indispensable considering the presence of CUS in the MOFs. For MIL-100(Al), all the unsaturated sites were occupied as evidenced by ^{27}Al NMR (see later discussion) [36], while the nature of the terminal groups (–F/–OH/–OH_2^+) is dependent on the synthesis conditions. The highly porous three-dimensional framework (S_{BET} up to 3100 m^2·g^{-1}, $V_p \approx 1.2$ cm^3·g^{-1}) possesses two types of mesoporous cages created by the assembly of supertetrahedra (25 and 29 Å) accessing through microporous windows of 4.7 × 5.4 and 8.8 Å (Fig. S1) [33–35]. It is worth mentioning that both the mesoporous cages and the micropore window allow uranyl ions to freely diffuse into the MOF, thus facilitating the U(VI) uptake in it.

3.2 Physicochemical properties of MIL-100s (Al, Cr, Fe)

The results of characterization of the as-synthesized MIL-100s are shown in Fig. 1. According to the PXRD patterns, the tested MIL-100s have the same skeleton topology and Bragg peaks with the simulated file (Fig. 1(a)) except for some changes in intensity which may result from different synthesis conditions. As the three MOFs (MIL-100s (Al, Fe, Cr)) were synthesized under harsh conditions, the water stability of these MOFs could be anticipated. After exposure in 0.1 mol·L^{-1} HCl solution for 24 h, for example, the framework of all the three MOFs keep stable as evidenced by PXRD in Fig. S2 (cf. ESM). The three materials can also maintain a high degree of crystallinity after uranium adsorption which verifies the high stability of the structure of MIL-100s (Fig. S3, cf. ESM). Thermal analysis for the MOFs reveals that MIL-100(Al) is much more stable upon heating than MIL-100(Fe) and MIL-100(Cr) (Fig. 1(b)). The initial weight loss (< 300 °C for MIL-100s (Fe, Cr) and < 500 °C for MIL-100(Al)) was attributed to the departures of free and bound water in the framework, followed by decomposition of the ligands. The thermal stability decreased in the order of MIL-100(Al) > MIL-100(Cr) > MIL-100(Fe) with the final products of Al_2O_3, Cr_2O_3 and Fe_2O_3, respectively. This degradation tendency is in line with the strength of metal–oxygen bond in Al_2O_3, Cr_2O_3, and Fe_2O_3 and thus can be rationalized by the strength of metal–oxygen bond in the MOFs [37]. The N_2 sorption isotherm on the fully evacuated analogous MIL-100 samples (Fig. 1(c)) showed clear type I nature with a slight secondary uptake, indicating the presence of micropores in these MOFs. The three MOFs have similar Langmuir surface area from 1670 to 1980 m^2·g^{-1}, and similar pore volume from 0.78 to 0.90 cm^3·g^{-1}, respectively (Table S1, cf. ESM), which is in agreement with the isostructuralism of these MOFs. Moreover, the large specific surface area is highly advantageous for uptake of metal ions since enough contact of metal ions with the sorbents is guaranteed.

3.3 Screening of MIL-MOFs for sequestration of U(VI) ions

The adsorptivity of MOFs materials towards U(VI) ions in aqueous solution had been investigated, as shown in

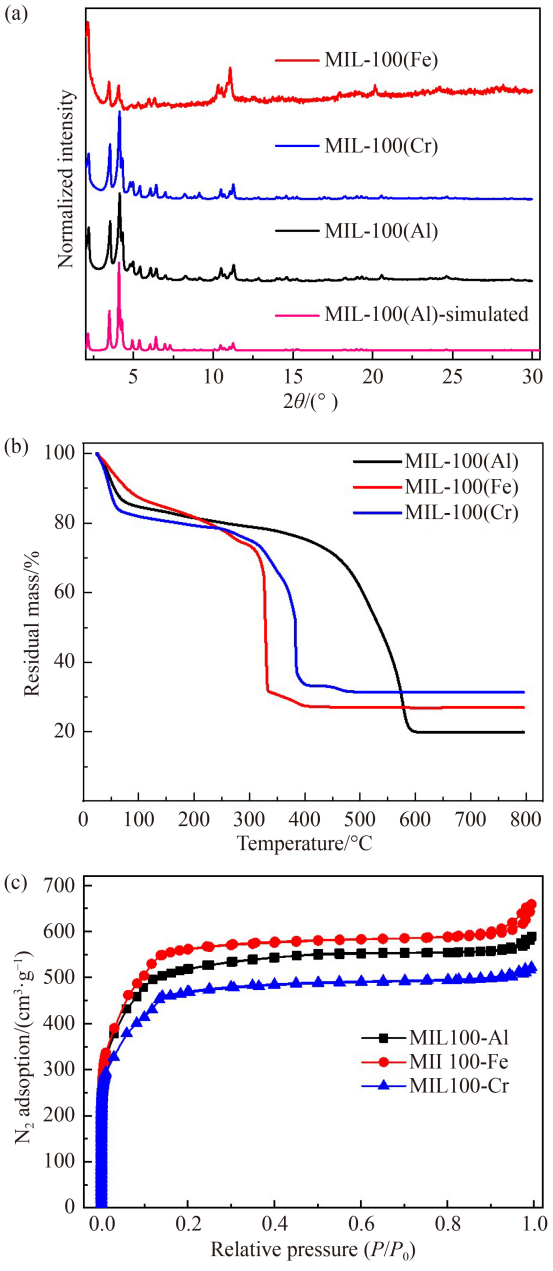

Fig. 1 Characterizations of the MIL-100 samples. (a) PXRD patterns; (b) TGA curves; (c) N_2 adsorption and desorption isotherms.

Fig. 2. For the sake of comparison, MIL-101(Cr) [38] (containing similar Cr_3O-nodes with MIL-100(Cr) and bridged by 1,4-benzene-dicarboxylate linkers, Fig. S1) and MIL-96(Al) [39] (with the same precursor materials as MIL-100(Al), Fig. S1) were also synthesized and tested as U(VI) sorbents. The results (Fig. 2(a)) showed that for the two Cr-based MOFs, i.e., MIL-101(Cr) and MIL-100(Cr), almost no U(VI) uptake occurred regardless of the topologies. For the two Al-based MOFs, however, the U(VI) uptake in MIL-100(Al) was 10 times larger than that in MIL-96(Al) at the same condition, which verifies the visible effect of the topology. This result also suggests that the U(VI) uptake in MOF sorbents is both metal node and topology dependent. The topology dependence (Fig. S4, cf. ESM) can be rationalized by the fact that MIL-100(Al) has more open pore structure and larger accessible pore volume than MIL-96(Al) (Fig. S1) and consequentially a higher U(VI) uptake. The effect of metal node, however, cannot be rationalized easily. This inspired us to characterize the relationship between the metal node of MOFs and the mechanism of MOFs in the realm of U(VI) uptake. To achieve this aim, considering that these MOFs have the same topology but different metal nodes, the U(VI) uptake in MIL-100s (Cr, Fe, Al) was further investigated.

3.3.1 Effect of pH

Solution pH is an important parameter for solid phase extraction of U(VI) ions due to both pH-dependent speciation of U(VI) and pH-dependent surface charge of sorbent. Herein, the pH effect was assessed by U(VI) uptake in MIL-100s (Al, Fe, Cr) at pH values ranging from 2.0 to 6.0 with an initial U(VI) concentration of 100 $mg \cdot L^{-1}$. The result is shown in Fig. 2(b). It is apparent that the U(VI) uptake into the three MOFs is highly pH dependent. In the tested pH range, the amount of U(VI) uptake greatly grew with the increase of the solution pH. The extremely low U(VI) uptake at low pH can be attributed to the positive charged surface of the MOFs as evidenced by zeta potential measurement, and the presence of excessive H^+ in MOFs that can compete with U(VI) to interact with the sorbent. When the solution pH increases, the electrostatic repulsion between U(VI) and the sorbent surface decreases and less H^+ ions are available to compete with the U(VI) for active binding sites, thus allowing the U(VI) uptake to increase. Besides, the speciation of U(VI) is also responsible for the pH-dependent U(VI) uptake. According to our previous works, the distribution of U(VI) species shows clear dependency on both pH values and U(VI) total concentration (Fig. S5, cf. ESM). At pH > 5.0 and U(VI) concentration of 5.0×10^{-5} $mol \cdot L^{-1}$, for example, UO_2^{2+} underwent hydrolysis, and multinuclear hydroxide complexes were the dominant species. These multinuclear hydroxides may be more favored by the MOF sorbents, thus leading to a pH-induced increase of the U(VI) uptake. In addition to demonstrating the pH-dependence, the data in Fig. 2(b) clearly show different performance of the three MOFs in the U(VI) uptake at various pH. For MIL-100(Al), the U(VI) uptake greatly increased when the pH value changed from 2 to 4 and then almost reached a plateau at pH > 4. By contrast, for MIL-100s (Fe, Cr), the U(VI) uptake slowly increased before a sharp rise at pH > 4. Such a result seems to give a hint that the U(VI) uptake in the three MOFs involves different mechanism, which will be discussed in detail in the last section.

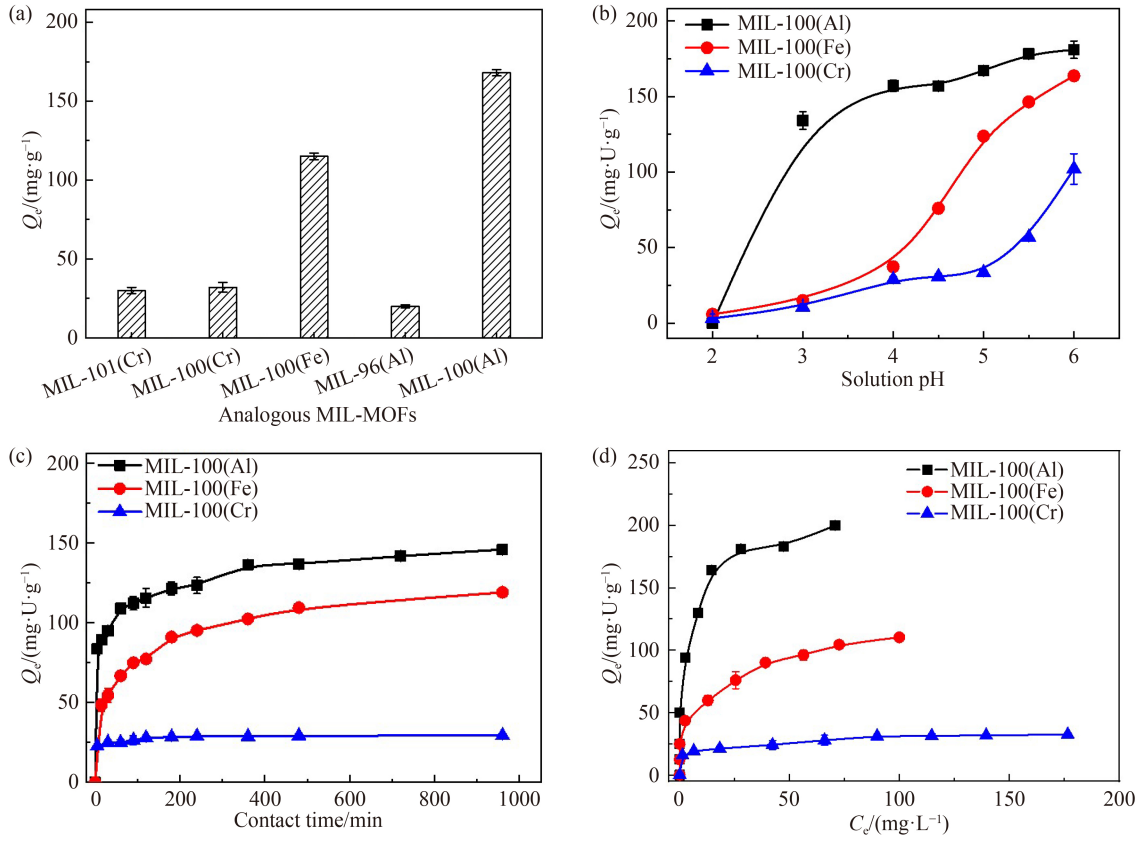

Fig. 2 The U(VI) uptake in MOFs. (a) Bar graph illustrating the adsorption capacities in several analogous MIL-MOFs (pH = 5 ± 0.1; t = 360 min; $m_{sorbent}/V_{solution}$ = 0.4 mg·mL^{-1}; $[U]_{initial}$ = 100 mg·L^{-1}). (b) pH dependence (t = 360 min; $m_{sorbent}/V_{solution}$ = 0.4 mg·mL^{-1}; $[U]_{initial}$ = 100 mg·L^{-1}). (c) Sorption kinetics (pH = 5 ± 0.1; $m_{sorbent}/V_{solution}$ = 0.4 mg·mL^{-1}; $[U]_{initial}$ = 100 mg·L^{-1}). (d) Sorption isotherms (pH = 5 ± 0.1; t = 360 min; $m_{sorbent}/V_{solution}$ = 0.4 mg·mL^{-1}).

3.3.2 Adsorption kinetics

To determine the sorption rate, the U(VI) sorption kinetics onto the three isostructural MIL-100s (Al, Fe, Cr) was performed at a time range of 5–960 min. As shown in Fig. 2(c), the sorption amounts of U(VI) on the three MOFs increased rapidly at the first 10 min and then reached equilibrium for MIL-100(Cr) and further increased slowly for MIL-100s (Al, Fe) until equilibrium at 6 h. The fast U(VI) sorption at the initial stage can be attributed to the rapid diffusion of U(VI) caused by the porous structure of the sorbents, and slow U(VI) sorption at the second stage for MIL-100s (Al, Fe) is related to chemisorption. Given the lack of the sorption sites, it is understandable that no further U(VI) sorption occurred for MIL-100(Cr) after 10 min.

To further understand the sorption kinetics. Pseudo-first-order [40] and pseudo-second-order [41] kinetics models were used to analyze the sorption data. The kinetic parameters and correlation coefficients are summarized in Fig. S6 (cf. ESM) and Table S2 (cf. ESM). For MIL-100(Al) and MIL-100(Fe), the pseudo-second-order model matches well with the experimental data with a high correlation coefficient of more than 0.99. The q_e values calculated by the model are very close to the experimentally observed equilibrium data, which indicates that the U(VI) sorption onto MIL-100s (Al, Fe) involves a chemisorption process. For MIL-100(Cr), it makes no sense to discuss much about the fitting result since the U(VI) uptake is too low.

3.3.3 Sorption isotherms

To further characterize the trend of U(VI) uptake onto the three isostructural MIL-100s, the sorption isotherms of U(VI) onto these MOFs at the various initial U(VI) concentration ($[U]_{initial}$) from 5 to 200 mg·L^{-1} was performed at room temperature with a constant contact time of 6 h. The results are shown in Fig. 2(d). It can be seen that although little U(VI) sorption (less than 35 mg·g^{-1}) onto MIL-100(Cr) occurred at the whole range of C_e, the U(VI) uptake onto MIL-100s (Al, Fe) increased rapidly with C_e increasing from 5 to 100 mg·L^{-1} and the increase slowed appreciably until the sorption saturation was maintained at C_e =150 mg·L^{-1}. Sorption capacities up to 210 and 115 mg of U(VI) per gram of MOFs were observed for MIL-100(Al) and MIL-100(Fe), respectively. These values are clearly higher than that observed for MIL-100(Cr). That is, the U(VI) uptake onto the three isostructural MIL-100s follows a clear trend of

MIL-100(Al) > MIL-100(Fe) > MIL-100(Cr).

To better understand the sorption mode of U(VI) in these MOF sorbents, two commonly used models, i.e., Langmuir isotherm [42,43] and Freundlich isotherm [34,42] model, were applied to fit the sorption data. The fitting plots as well as parameters obtained from the models are presented in Fig. S7 (cf. ESM) and Table S3 (cf. ESM). Based on the value of the correlation coefficient (R^2), it could be concluded that Langmuir model rather than Freundlich model is suitable to describe the U(VI) sorption onto MIL-100(Al) and MIL-100(Fe), designating a monolayer uniform sorption mode. The maximum sorption capacities up to 212.8 and 116.3 mg U(VI) per gram of MOFs were calculated for MIL-100(Al), and MIL-100(Fe), respectively, corresponding to 0.5 and 0.32 uranyl ions adsorbed per node in the MOFs, respectively (Table S4, cf. ESM). For MIL-100(Cr), the sorption data fits well with both the Langmuir and Freundlich models (R^2 > 0.99), suggesting a complex sorption mode. Again, it makes no sense to discuss much about the fitting result since the U(VI) uptake is too low.

3.3.4 Effect of ion strength

Given that wastewater always contains various kinds of ions, the ability to maintain high efficiencies towards specific metal ions even at high ionic strength is one of the most important factors when evaluating a sorbent for water treatment applications, as shown in Fig. 3. Herein, the effect of ionic strength on U(VI) uptake by these MOF sorbents was assessed by varying $NaClO_4$ concentration from 0.1 to 1 mol·L^{-1}, and the results were compared with that in the absence of $NaClO_4$ (Fig. 3(a)). It is clear that at low $NaClO_4$ concentration of less than 0.2 mol·L^{-1}, the U(VI) uptake in all the three MOFs was independent of ionic strength related to the $NaClO_4$ concentration. When the $NaClO_4$ concentration was further increased, the amount of U(VI) sorbed in MIL-100(Fe) and MIL-100(Cr) still kept constant, whereas for MIL-100(Al), an abnormal increase of U(VI) uptake was observed. The ionic strength independent sorption can be rationalized from the viewpoint of complexation. That is, inner-sphere complexation occurs during the U(VI) sorption in the MOF sorbents, which is consistent with previously reported work [44] and also can be evidenced by the ^{27}Al NMR characterization (see later discussion). Besides, we concluded that the abnormal increase of U(VI) uptake is mainly attributed to the ion exchange between U(VI) and Na^+ and/or the electrostatic interaction between U(VI) and ClO_4^- (see later discussion). Whatever, the above results are interesting and important. At $NaClO_4$ concentration of 1 mol·L^{-1}, the mole ration of Na^+ to U(VI) is ca. 2380. Despite this, the MOF sorbents maintain high sorption efficiencies towards U(VI), reflecting excellent anti-interference ability of these materials.

3.3.5 Effect of competing cations

Encouraged by the results above, we then assessed selectivity of these MOFs towards U(VI) over common metal cations. Given that alkaline earth metal ions, transition metal ions and rare earth metal ions always occur as common cations in various wastewaters, the selectivity test was carried out using a solution containing Zn^{2+}, Cr^{3+}, Pb^{2+}, Sr^{2+}, Ni^{2+}, Co^{2+}, Yb^{3+}, and UO_2^{2+}, in which the concentration of all the metal ions was identical to 0.5 mmol·L^{-1}. The results are shown in Fig. 3(b). The adsorption performance of MIL-100(Cr) for uranium does not exceed 40 mg·g^{-1} at pH 5.0, so it is not meaningful to discuss the selectivity of this MOF. Therefore, only the selectivity of MIL-100(Al) and MIL-100(Fe) is discussed below. As can be seen, at pH 5.0, both MIL-100(Fe) and MIL-100(Al) maintained very high sorption efficiencies towards U(VI) with uptake amount of 101 and 149 mg·g^{-1}, respectively. These values are comparable with that in the single metal sorption experiments (120 and 165 mg·g^{-1},

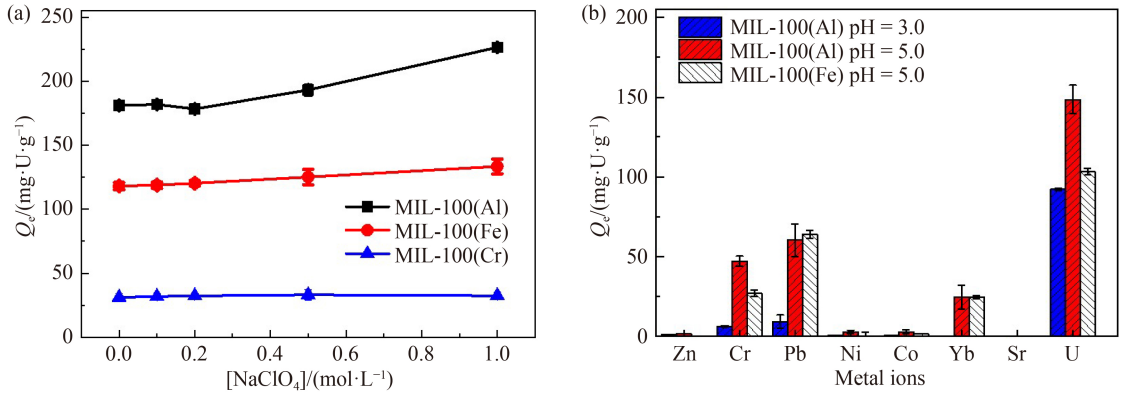

Fig. 3 (a) Effect of ionic strength (pH = 5 ± 0.1; t = 360 min; $m_{sorbent}/V_{solution}$ = 0.4 mg·mL^{-1}; $[U]_{initial}$ = 100 mg·L^{-1}); (b) competing cations on U(VI) uptake in MIL-100s (Al, Fe, Cr). The concentration of all metal ions was 0.5 mmol·L^{-1}. $m_{sorbent}/V_{solution}$ = 0.4 mg·mL^{-1}; pH = 5 ± 0.1; t = 360 min.

respectively), which further confirms the excellent anti-interference ability of these MOF sorbents. However, besides U(VI), a certain amount of Cr^{3+}, Yb^{3+} and Pb^{2+} were simultaneously sorbed at such a pH. For Pb^{2+}, for example, the sorption amount in MIL-100(Al) reached 60 $mg \cdot g^{-1}$. When pH was decreased to 3.0, however, a high U(VI) uptake of 92 $mg \cdot g^{-1}$ in MIL-100(Al) was maintained. By contrast, almost no other metal ions including Pb^{2+} were sorbed, suggesting the excellent selectivity of the MOFs towards U(VI). In other words, the MOF sorbents show desirable selectivity towards U(VI) at a lower pH.

3.4 Mechanism proposal

Generally speaking, physical sorption or chemical bonding or both contribute to metal ion uptake onto a specific sorbent, depending on the type of interaction between sorbent and adsorbate [45]. To understand the U(VI) sorption mode onto MIL-100s (Al, Fe, Cr), these pristine MOFs and the U(VI)-loaded samples had been comparatively characterized (Fig. 4). Figure 4(a) shows the zeta potential of the three MOFs as function of solution pH. As can be seen, the surface charge for all the three MOFs became more negative with the increase of pH. The point of zero charge (pH_{pzc}) values of 5.8, 4.2 and 3.5 were observed for MIL-100(Al), MIL-100(Fe), and MIL-100(Cr), respectively [46]. That is, at the same pH, MIL-100(Cr) shows the most negative charged surface among the three MOFs, while MIL-100(Al) is the least. This result is opposite to what would be expected from the sorption capacities (Fig. S8, cf. ESM), which clearly suggests that electrostatic attraction is not the reason for the U(VI) sorption onto MIL-100(Al) and MIL-100(Fe), although it is likely the main mechanism for MIL-100(Cr).

We then turned our attention to the functional groups on the surface of the MOFs. As is well known, MIL-100s present abundant of coordinated unsaturated sites, which necessitates the hydroxo or aquo groups to complete the metal-coordination sphere, thus forming terminal hydroxyl groups (≡S–OH) [47,48] (S here represents metal node of MIL-100). It is documented that the terminal groups can be easily removed and the unsaturated sites are re-exposed following high-temperature vacuum heating [36], leading to a peak between 25 and 40 ppm (10^{-6}) on solid ^{27}Al NMR related to 5-coordinated aluminum species [35,36]. Under the conditions of synthesis and sorption in this work, however, there is no ^{27}Al NMR peaks in the range of 25–40 ppm (Fig. 4(b)), indicating that the terminal hydroxyl groups always occur in the surface of MIL-

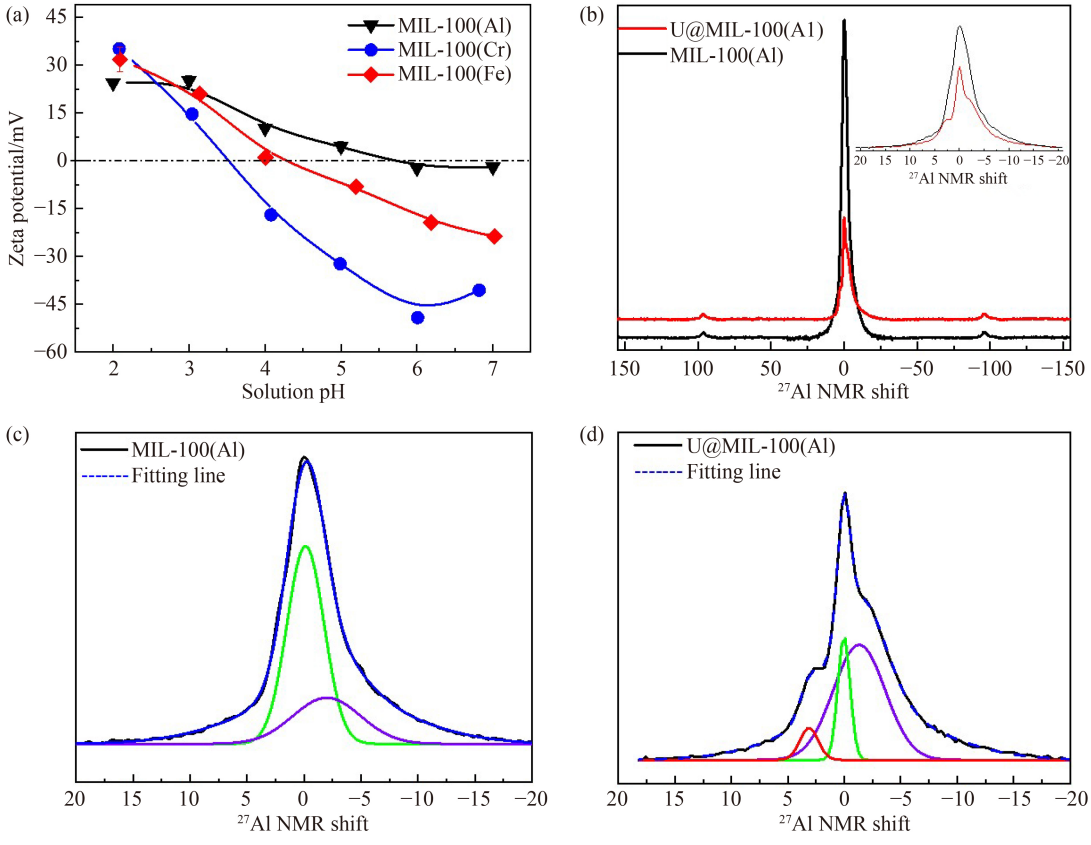

Fig. 4 (a) Zeta Potential of MIL-100; (b) ^{27}Al NMR spectra of pristine MIL-100(Al) (dark line) and after uranyl ion adsorption (red line); (c) fitting line of ^{27}Al NMR spectra of pristine MIL-100(Al); (d) after adsorption of U(VI).

100(Al) and act as functional groups. These surface hydroxyl groups undergo protonation and deprotonation as follows depending on the ambient environments, which contributes to U(VI) uptake in different ways.

$$\equiv SOH + H^+ \leftrightarrow \equiv SOH_2^+ \quad (3)$$

$$\equiv SO^-H^+ \leftrightarrow \equiv SO^- + H^+ \quad (4)$$

At a lower pH, for example pH < 5.0, the protonation of the hydroxyl groups in the MOF surface occurs. As an evidence, the pH of the reaction solution during synthesis of MIL-100(Al) is gradually increased from 0.57 to 1.85, suggesting that a considerable amount of H^+ was sorbed by the MOFs. As another evidence, MIL-100(Al) exhibits positively charged surface until pH 5.8 (Fig. 4(a)) until pH_{pzc} is reached. Since MIL-100(Al) efficiently sorb U(VI) in the pH range of 2–5.8 (Fig. 2(b)), we consider that the mechanism involves direct exchange of U(VI) cation with H^+ as follows:

$$\equiv Al - OH_2^+ + M^+ \leftrightarrow \equiv Al - OH - M^+ + H^+ \quad (5)$$

where M^+ denotes U(VI) cation in the form of UO_2^{2+} hydrate and hydroxide complex such as $(UO_2)_2(OH)_2^{2+}$ and $(UO_2)_3(OH)_5^+$. In this case, as pH increases, the reduction of H^+ in solution promotes the exchange balance from left to right, thus leading to an enhanced U(VI) uptake. Moreover, when sodium ions (Na^+) are present in the system, for example, in the ion strength experiment, the H^+ in the MOF surface is initially replaced by Na^+ and then the Na^+ is exchanged by U(VI) cation:

$$\equiv SO^-H^+ + Na^+ \leftrightarrow \equiv SO^-Na^+ + H^+ \quad (6)$$

$$\equiv SO^-Na^+ + M^+ \leftrightarrow \equiv SO^-M^+ + Na^+ \quad (7)$$

The formation of ion pairs facilitates the exchange of U(VI) cations into the MOFs, thus resulting in an abnormal increase of U(VI) uptake with the rise of ion strength (Fig. 3(a)).

At a middle pH, such as pH 5–6, there is no too many exchangeable H^+ since it is near pH_{pzc} of MIL-100(Al). At this time, it is believed that the U(VI) uptake in MIL-100(Al) occurs through coordination between the surface hydroxyl groups and U(VI). To confirm this, ^{27}Al NMR spectra for MIL-100(Al) (Figs. 4(b–d)) before and after U(VI) were recorded and compared. It is found that the NMR peak of MIL-100(Al) remained intact as a whole following U(VI) uptake, but a new peak of Al at 3 ppm appears as shown in Figs. 4(c) and 4(d). This result gives a hint that there is strong interaction between the Al and uranyl ion, which results in the charge transfer of Al species and consequentially causes part of the Al peak to move to the high field in the ^{27}Al NMR. In other words, the inner-sphere U(VI) complexes are formed on the surface of MIL-100(Al) under in this pH region. The coordination interaction clearly enhances the affinity of MOFs towards U(VI), thus yielding sharper isotherm curves of MIL-100(Al) at lower uranyl equilibrium concentrations (Fig. 2(d)).

At a higher pH, such as pH > 6, all the three MOFs show negatively charged surface, which is probably resulted from the deprotonation of the surface hydroxyl groups (Eq. (8)). Besides, it is reported that the Cr-center metal cluster in MIL-101(Cr) dissociates protons from the water ligand ($Cr–OH_2$) leaving a negatively charged hydroxyl group ($Cr–OH^-$) [49]. In this case, whatever, the U(VI) uptake mainly occurs through electrostatic attraction between negatively charged surface and positive U(VI) ions until U(VI) ions become negative species at a higher pH:

$$\equiv S - OH \leftrightarrow \equiv S - O^- + H^+ \quad (8)$$

$$\equiv Cr - OH_2 \leftrightarrow \equiv Cr - OH^- + H^+ \quad (9)$$

Considering all of the above discussions, it is apparent that the overall sorption of U(VI) onto MIL-100s (Cr, Fe, Al) must be described by a combination of three processes: ion exchange (Eqs. (5)–(7)), coordination interaction, and electrostatic attraction. Their relative importance is determined by the aqueous acidity, ionic strength, and metal node of the MOFs. To the best of our knowledge, such a ternary (i.e., three-path) sorption mechanism has rarely counterpart in traditional solid-phase extraction systems employing functional porous materials as metal ions sorbents. This is also one of the few studies on the effect of open metal sites on the adsorptivity of MOFs towards metal ions.

4 Conclusions

Taking U(VI) sorption onto MIL-100s (Al, Fe, Cr) as examples, for the first time, analogous MOFs for efficient water purification by tuning the center metal ions of the frameworks was reported. MIL-100(Al) shows good performance on U(VI) capture from aqueous solution with rapid kinetics and high capacities, while analogous MOFs MIL-100(Cr) is the worst. The findings of this work prove that not all of the MOFs crystals are efficient for sorption application due to the activity difference of terminal metal hydrates, and thus modulating the center metal ions of the frameworks provides an effective way to improve the sorption performance. The U(VI) uptake on the three MOFs was confirmed to involve a ternary (i.e., three-path) sorption mechanism, i.e., ion exchange, coordination interaction, and electrostatic attraction, which has rarely counterpart in traditional solid-phase extraction systems employing functional porous materials as metal ions sorbents. This work offers a new strategy for designing highly-efficient sorbents by varying metal ions/clusters of MOFs, which is also helpful to better understand the correlation between the structure and activity of MOFs as a sorbent. On the other hand, however, this work also leads to some new issues such as

origins of the activity difference of terminal metal hydrates in MOFs. Therefore, computational efforts in our laboratory being focused on those challenging unknowns are in progress.

Acknowledgements This work was supported by the National Natural Science Foundation of China (Grant Nos. U20B2019, 21790373 and 21790370) and the National Science Fund for Distinguished Young Scholars (Grant No. 21925603).

Electronic Supplementary Material Supplementary material is available in the online version of this article at https://dx.doi.org/10.1007/s11705-022-2187-6 and is accessible for authorized users.

References

1. Dresselhaus M S, Thomas I L. Alternative energy technologies. Nature, 2001, 414(6861): 332–337
2. Whitfield S C, Rosa E A, Dan A, Dietz T. The future of nuclear power: value orientations and risk perception. Risk Analysis, 2009, 29(3): 425–437
3. Chakravarty R, Dash A. Nanomaterial-based adsorbents: the prospect of developing new generation radionuclide generators to meet future research and clinical demands. Journal of Radioanalytical and Nuclear Chemistry, 2013, 299(1): 741–757
4. Yang D X, Song S, Zou Y D, Wang X X, Yu S J, Wen T, Wang H Q, Hayat T, Alsaedi A, Wang X K. Rational design and synthesis of monodispersed hierarchical SiO_2@layered double hydroxide nanocomposites for efficient removal of pollutants from aqueous solution. Chemical Engineering Journal, 2017, 323: 143–152
5. Wang X X, Chen L, Wang L, Fan Q H, Pan D Q, Li J X, Chi F T, Xie Y, Yu S J, Xiao C L, Luo F, Wang J, Wang X, Chen C, Wu W, Shi W, Wang S, Wang X. Synthesis of novel nanomaterials and their application in efficient removal of radionuclides. Science China Chemistry, 2019, 62(8): 933–967
6. Yu J P, Yuan LY, Wang S, Lan J H, Zheng L R, Xu C, Chen J, Wang L, Huang Z W, Tao W Q, Liu Z R, Chai Z F, Gibson J K, Shi W Q. Phosphonate-decorated covalent organic frameworks for actinide extraction: a breakthrough under highly acidic conditions. CCS Chemistry, 2019, 1(3): 286–295
7. Ahmad Z, Li Y, Ali S, Yang J J, Jan F, Fan Y, Gou X Y, Sun Q Y, Chen J P. Benignly-fabricated supramolecular poly(amidoxime)-alginate-poly(acrylic acid) beads synergistically enhance uranyl capture from seawater. Chemical Engineering Journal, 2022, 441: 136076
8. Ahmad Z, Li Y, Yang J J, Geng N B, Fan Y, Gou X Y, Sun Q Y, Chen J P. A membrane-supported bifunctional poly(amidoxime-ethyleneimine) network for enhanced uranium extraction from seawater and wastewater. Journal of Hazardous Materials, 2022, 425: 127995
9. Xie Y, Chen C L, Ren X M, Wang X X, Wang H Y, Wang X K. Emerging natural and tailored materials for uranium-contaminated water treatment and environmental remediation. Progress in Materials Science, 2019, 103: 180–234
10. Zhang N, Peng W T, Guo H, Wang H H, Li Y, Liu J, Zhang S L, Mei P, Hayat T, Sun Y. Fabrication of porous carbon and application of Eu(III) removal from aqueous solutions. Journal of Molecular Liquids, 2019, 280: 34–39
11. Zheng B N, Lin X D, Zhang X C, Wu D C, Matyjaszewski K. Emerging functional porous polymeric and carbonaceous materials for environmental treatment and energy storage. Advanced Functional Materials, 2019, 30(41): 1907006
12. Kim C, Lee S S, Kwan K T, Lee J, Li W, Lafferty B J, Giammar D E, Fortner J D. Surface functionalized nanoscale metal oxides for arsenic(V), chromium(VI), and uranium(VI) sorption: considering single- and multi-sorbate dynamics. Environmental Science: Nano, 2020, 7(12): 3805–3813
13. Li K D, Xiong T, Liao J, Lei Y Q, Zhang Y, Zhu W K. Design of MXene/graphene oxide nanocomposites with micro-wrinkle structure for efficient separating of uranium(VI) from wastewater. Chemical Engineering Journal, 2022, 433: 134449
14. Liu T, Zhang R Q, Chen M W, Liu Y J, Xie Z J, Tang S, Yuan Y H, Wang N. Vertically aligned polyamidoxime/graphene oxide hybrid sheets' membrane for ultrafast and selective extraction of uranium from seawater. Advanced Functional Materials, 2021, 32(14): 2111049
15. Boulanger N, Kuzenkova A S, Iakunkov A, Romanchuk A Y, Trigub A L, Egorov A V, Bauters S, Amidani L, Retegan M, Kvashnina K O, Kalmykov S N, Talyzin A V. Enhanced sorption of radionuclides by defect-rich graphene oxide. ACS Applied Materials & Interfaces, 2020, 12(40): 45122–45135
16. Jana A, Unni A, Ravuru S S, Das A, Das D, Biswas S, Sheshadri H, De S. *In-situ* polymerization into the basal spacing of LDH for selective and enhanced uranium adsorption: a case study with real life uranium alkaline leach liquor. Chemical Engineering Journal, 2022, 428: 131180
17. Guo X L, Ruan Y, Diao Z H, Shih K, Su M H, Song G, Chen D Y, Wang S, Kong L J. Environmental-friendly preparation of Ni–Co layered double hydroxide (LDH) hierarchical nanoarrays for efficient removing uranium(VI). Journal of Cleaner Production, 2021, 308: 127384
18. Chen Z, Mian M R, Lee S J, Chen H, Zhang X, Kirlikovali K O, Shulda S, Melix P, Rosen A S, Parilla P A, Gennett T, Snurr R Q, Islamoglu T, Yildirim T, Farha O K. Fine-tuning a robust metal–organic framework toward enhanced clean energy gas storage. Journal of the American Chemical Society, 2021, 143(45): 18838–18843
19. Zhang Y F, Zhang Z H, Ritter L, Fang H, Wang Q, Space B, Zhang Y B, Xue D X, Bai J. New reticular chemistry of the rod secondary building unit: synthesis, structure, and natural gas storage of a series of three-way rod amide-functionalized metal–organic frameworks. Journal of the American Chemical Society, 2021, 143(31): 12202–12211
20. Gong W, Xie Y, Pham T D, Shetty S, Son F A, Idrees K B, Chen Z, Xie H, Liu Y, Snurr R Q, Chen B, Alameddine B, Cui Y, Farha O K. Creating optimal pockets in a clathrochelate-based metal-organic framework for gas adsorption and separation: experimental and computational studies. Journal of the American Chemical Society, 2022, 144(8): 3737–3745
21. Pei J, Gu X W, Liang C C, Chen B, Li B, Qian G. Robust and radiation-resistant hofmann-type metal–organic frameworks for

record xenon/krypton separation. Journal of the American Chemical Society, 2022, 144(7): 3200–3209
22. Shu L, Peng Y, Yao R, Song H L, Zhu C Y, Yang W S. Flexible soft-solid metal–organic framework composite membranes for H_2/CO_2 separation. Angewandte Chemie International Edition, 2022, 61(14): e202117577
23. Moumen E, Bazzi L, El Hankari S. Metal–organic frameworks and their composites for the adsorption and sensing of phosphate. Coordination Chemistry Reviews, 2022, 455: 214376
24. Platero-Prats A E, Mavrandonakis A, Liu J, Chen Z, Chen Z, Li Z, Yakovenko A A, Gallington L C, Hupp J T, Farha O K, Cramer C J, Chapman K W. The molecular path approaching the active site in catalytic metal–organic frameworks. Journal of the American Chemical Society, 2021, 143(48): 20090–20094
25. Mallakpour S, Nikkhoo E, Hussain C M. Application of MOF materials as drug delivery systems for cancer therapy and dermal treatment. Coordination Chemistry Reviews, 2022, 451: 214262
26. Carboni M, Abney C W, Liu S, Lin W. Highly porous and stable metal–organic frameworks for uranium extraction. Chemical Science (Cambridge), 2013, 4(6): 2396
27. Bai Z Q, Yuan L Y, Zhu L, Liu Z R, Chu S Q, Zheng L R, Zhang J, Chai Z F, Shi W Q. Introduction of amino groups into acid-resistant MOFs for enhanced U(VI) sorption. Journal of Materials Chemistry A, 2015, 3(2): 525–534
28. Zhang N, Yuan L Y, Guo W L, Luo S Z, Chai Z F, Shi W Q. Extending the use of highly porous and functionalized MOFs to Th(IV) capture. ACS Applied Materials & Interfaces, 2017, 9(30): 25216–25224
29. Yuan L Y, Tian M, Lan J H, Cao X Z, Wang X L, Chai Z F, Gibson J K, Shi W Q. Defect engineering in metal–organic frameworks: a new strategy to develop applicable actinide sorbents. Chemical Communications (Cambridge), 2018, 54(4): 370–373
30. Yoon J W, Chang H, Lee S J, Hwang Y K, Hong D Y, Lee S K, Lee J S, Jang S, Yoon T U, Kwac K, Jung Y, Pillai R S, Faucher F, Vimont A, Daturi M, Férey G, Serre C, Maurin G, Bae Y S, Chang J S. Selective nitrogen capture by porous hybrid materials containing accessible transition metal ion sites. Nature Materials, 2017, 16(5): 526–531
31. Tong M M, Liu D H, Yang Q Y, Devautour-Vinot S, Maurin G, Zhong C L. Influence of framework metal ions on the dye capture behavior of MIL-100 (Fe, Cr) MOF type solids. Journal of Materials Chemistry A, 2013, 1(30): 8534
32. Zhang Z H, Lan J H, Yuan L Y, Sheng P P, He M Y, Zheng L R, Chen Q, Chai Z F, Gibson J K, Shi W Q. Rational construction of porous metal–organic frameworks for uranium(VI) extraction: the strong periodic tendency with a metal node. ACS Applied Materials & Interfaces, 2020, 12(12): 14087–14094
33. Férey G, Serre C, Mellot-Draznieks C, Millange F, Surblé S, Dutour J, Margiolaki I. A hybrid solid with giant pores prepared by a combination of targeted chemistry, simulation, and powder diffraction. Angewandte Chemie International Edition, 2004, 43(46): 6296–6301
34. Horcajada P, Surble S, Serre C, Hong D Y, Seo Y K, Chang J S, Greneche J M, Margiolaki I, Ferey G. Synthesis and catalytic properties of MIL-100(Fe), an iron(III) carboxylate with large pores. Chemical Communications (Cambridge), 2007, 27(27): 2820–2822
35. Volkringer C, Popov D, Loiseau T, Férey G R, Burghammer M, Riekel C, Haouas M, Taulelle F. Synthesis, single-crystal X-ray microdiffraction, and NMR characterizations of the giant pore metal–organic framework aluminum trimesate MIL-100. Chemistry of Materials, 2009, 21(24): 5695–5697
36. Haouas M, Volkringer C, Loiseau T, Férey G, Taulelle F. Monitoring the activation process of the giant pore MIL-100(Al) by solid state NMR. Journal of Physical Chemistry C, 2011, 115(36): 17934–17944
37. Low J J, Benin A I, Jakubczak P, Abrahamian J F, Faheem S A, Willis R R. Virtual high throughput screening confirmed experimentally: porous coordination polymer hydration. Journal of the American Chemical Society, 2009, 131(43): 15834–15842
38. Hwang Y K, Hong D Y, Chang J S, Jhung S H, Seo Y K, Kim J, Vimont A, Daturi M, Serre C, Ferey G. Amine grafting on coordinatively unsaturated metal centers of MOFs: consequences for catalysis and metal encapsulation. Angewandte Chemie International Edition, 2008, 47(22): 4144–4148
39. Loiseau T, Lecroq L, Volkringer C, Marrot J, Férey G, Haouas M, Taulelle F, Bourrelly S, Llewellyn P, Latroche M. MIL-96, a porous aluminum trimesate 3D structure constructed from a hexagonal network of 18-membered rings and μ 3-oxo-centered trinuclear units. Journal of the American Chemical Society, 2006, 128(31): 10223–10230
40. Yuan L Y, Liu Y L, Shi W Q, Lv Y L, Lan J H, Zhao Y L, Chai Z F. High performance of phosphonate-functionalized mesoporous silica for U(VI) sorption from aqueous solution. Dalton Transactions (Cambridge, England), 2011, 40(28): 7446–7453
41. Ho Y S, McKay G. The kinetics of sorption of divalent metal ions onto sphagnum moss peat. Water Research, 2000, 334(3): 735–742
42. Foo K Y, Hameed B H. Insights into the modeling of adsorption isotherm systems. Chemical Engineering Journal, 2010, 156(1): 2–10
43. Langmuir I. The adsorption of gases on plane surfaces of glass, mica and platinum. Journal of the American Chemical Society, 1918, 40(9): 1361–1403
44. Lützenkirchen J. Ionic strength effects on cation sorption to oxides: macroscopic observations and their significance in microscopic interpretation. Journal of Colloid and Interface Science, 1997, 15(1): 149–155
45. Jia W, Fang Y, Zeng G M. Progress and prospect of adsorptive removal of heavy metal ions from aqueous solution using metal–organic frameworks: a review of studies from the last decade. Chemosphere, 2018, 201: 627–643
46. Jun J W, Tong M, Jung B K, Hasan Z, Zhong C, Jhung S H. Effect of central metal ions of analogous metal–organic frameworks on adsorption of organoarsenic compounds from water: plausible mechanism of adsorption and water purification. Chemistry (Weinheim an der Bergstrasse, Germany), 2015, 21(1): 347–354
47. Lamb A C M, Grieser F, Healy T W. The adsorption of uranium(VI) onto colloidal TiO_2, SiO_2 and carbon black. Colloids and Surfaces A, 2016, 499: 156–162

48. Zou Y D, Wang X X, Wu F, Yu S J, Hu Y Z, Song W C, Liu Y H, Wang H Q, Hayat T, Wang X K. Controllable synthesis of Ca–Mg–Al layered double hydroxides and calcined layered double oxides for the efficient removal of U(VI) from wastewater solutions. ACS Sustainable Chemistry & Engineering, 2016, 5(1): 1173–1185
49. Herbst A, Khutia A, Janiak C. Bronsted instead of Lewis acidity in functionalized MIL-101Cr MOFs for efficient heterogeneous (nano-MOF) catalysis in the condensation reaction of aldehydes with alcohols. Inorganic Chemistry, 2014, 53(14): 7319–7333